The effects of anthropogenic greenhouse gases and aerosols on the inter-decadal change of the South China Sea summer monsoon in the late twentieth century

Article

Accepted Version

www.reading.ac.uk/centaur

CentAUR

Central Archive at the University of Reading

Reading's research outputs online

1 **The effects of anthropogenic greenhouse gases and aerosols on the inter-decadal change**

2 **of the South China Sea summer monsoon in the late 20th Century**

3 **Zhongxi Lin[1] Buwen Dong[2] Zhiping Wen[3]**

4 1 Center for Monsoon and Environment Research/School of Atmospheric Sciences, Sun Yat-sen

5 University, Guangzhou, China

6 2 Department of Meteorology, National Centre for Atmospheric Science, University of Reading,

7 Reading, UK

8 3 Department of Atmospheric and Oceanic Sciences & Institute of Atmospheric Sciences, Fudan

9 University, Shanghai, China

10

11

12

13

14

15

16

17

18

19 Corresponding author:

20 Zhongxi Lin,

21 Center for Monsoon and Environment Research/ School of Atmospheric Sciences

22 Sun Yat-Sen University,

23 Zhuhai, 519082 China

24 E-mail: linzhxi@mail2.sysu.edu.cn

26   **Abstract:** Analysis of observational precipitation indicates that in last few decades, the

27   precipitation in boreal summer (June-August) over the South China Sea (SCS) exhibited an

28   interdecadal variation, characterized by a decrease of 0.59mm/day from the period 1964-

29   1981 to the period 1994-2011. Accompanied this decrease in precipitation is weakened

30   monsoon circulation featured by an anti-cyclonic circulation anomaly over the SCS in the

31   later period relative to the early period. This work investigates impacts of anthropogenic

32   forcing changes on this interdecadal change in observations, quantify the relative roles of

33   greenhouse gases (GHG) forcing and anthropogenic aerosol (AA) forcing. A set of

34   experiments is designed using the atmospheric component of a state-of-the-art climate

35   model coupled to a multi-level mixed-layer ocean model forced with GHG concentrations

36   and AA emissions in two periods.   Modeling results indicate a dominant role of

37   anthropogenic forcing on the observed interdecadal precipitation decrease and weakened

38   monsoon circulation over the SCS in the late 20th century in which AA forcing plays a more

39   important role compared with GHG forcing. The mechanisms of GHG influences and AA

40   induced changes are revealed by individual forcing experiments. Increasing GHG

41   concentrations can suppress convection over the SCS summer monsoon (SCSSM) region

42   by warming the tropical Pacific with an El-Niño like sea surface temperature (SST) pattern,

43   which is associated with a weakened Walker circulation. The changes in AA emissions,

44   mainly through increases in emissions over Asia, lead to cool SST in the north Indian Ocean

45   and the western North Pacific (WNP), and result in changes in meridional SST gradient over

46   the tropical Indian Ocean and the WNP in pre-monsoon seasons. This anomalous

47   meridional SST gradient leads to anomalous local Hadley circulation, characterized by

48   anomalous ascents around the equator and descents over monsoon region, which

49   suppresses convection over the SCS and reduces local precipitation.

50   **Key words**: South China Sea summer monsoon, anthropogenic greenhouse gases,

51   anthropogenic aerosols, precipitation.

52

53   1 Introduction

54   The South China Sea (SCS) locates in Southeast Asia between the equator and South

55   China coast, from 110°E to 120°E. It is in the center of the Asian-Australian monsoon system

56   and has a close relation with the East Asian monsoon, South Asian monsoon and Western

57   North Pacific monsoon due to geographic location (Tao and Chen 1987; Ding 1992,

58   Murakami and Matsumoto 1994; Wang 1994; Lau and Yang 1997). The climate over the

59   SCS is mainly controlled by monsoon circulation, characterized by a warm and wet westerly

60   low-level flow during boreal summer, and cold and dry easterly low-level flow during winter.

61   In summer, westerly flow comes from the Indian Ocean, turns into southerly and transports

62   moisture to the East Asian monsoon region. Over the SCS, this cyclonic circulation forms a

63   local monsoon trough and leads to convection and abundant precipitation.

64   The SCS summer monsoon (SCSSM) changes in multiple time-scales (Zhou et al. 2005;

65   Wang et al. 2009; Tong et al. 2009) and can be affected by many different factors, including

66   solar radiation on orbital time scale (Prell 2011), interdecadal time scale, and sea surface

67   temperature (SST) variability and land-sea thermal contrast on interannual time scale (Wang

68   and Zhang 2002; Lau et al. 2004; Zhou et al. 2005; Lau and Wang 2006; Yuan et al. 2008;

69   Wang and Qian 2009; Zhu et al. 2011). Its intensity is sensitive to the definition since the

70   SCSSM can be affected by the multiple monsoon subsystems, including the East Asian

71   summer monsoon (EASM), South Asian summer monsoon (SASM), and western North

72 Pacific summer monsoon (WNPSM). Previous researches use some indices to describe

73 characteristics of the SCSSM, including its southwesterly low-level flow, local convection

74 and moisture transport convergence (Lu and Chan 1999; Liang et al. 1999; Li and Zhang

75 1999; Dai et al. 2000; Liang et al. 1999; Wu and Liang 2001; Yao and Qian 2001; Zhang et

76 al. 2002; Wen et al. 2006; Wang et al. 2008). A meridional shear vorticity index (zonal wind

77 in the south SCS minus that in the north SCS; Wang et al. 2009) is created to describe the

78 strength of the SCSSM and is then widely used. Based on 7-year mean of this index, inter-

79 decadal changes are observed in the early 1970s and the early 1990s (Wang et al. 2009).

80 However, drivers and physical mechanisms for these interdecadal changes are not fully

81 investigated.

82 The interdecadal variation of the EASM and SASM has been attributed to both internal

83 variability associated with low frequency SST variability in the Atlantic and Pacific (i.e., the

84 Pacific Decadal Oscillation [PDO] and the Atlantic Multidecadal Oscillation [AMO], Goswami

85 et al. 2006; Lu et al. 2006; Zhou et al. 2009) and external forcing associated with changes

86 in greenhouse gases (GHG) and anthropogenic aerosol (AA) emissions (Song et al. 2014;

87 Li et al. 2015; Li and Ting 2017, Tian et al. 2018, Luo et al. 2019). Most of previous studies

88 agree that precipitation tends to increase in both EASM and SASM due to increased

89 moisture content in the atmosphere with increasing GHG forcings. Despite of the increased

90 moisture content, the effect of GHG and AA on the monsoon circulation is important and

91 requires further research.

92 The greenhouse gases (GHG) can change the SASM monsoon circulation by changing

93 the large-scale tropical Walker circulations and land-sea thermal contrast (Ueda et al. 2005).

94 In some model studies, the intensity of the Walker circulation connecting the tropical Pacific

95 and monsoon region tends to be weakened (Tanaka et al. 2004; Ueda et al. 2005, May 2002,

96 Vecchi and Soden 2006; Lau and Kim 2017), which suppresses the convection in the SASM

97 region. The land-sea thermal contrast is increased as the temperature over land response

98 to GHG increases is stronger than over ocean (Sutton et al. 2007; Dong et al. 2009). The

99 land-sea thermal contrast between South Asia and Indian ocean, which is an important

100 driver of the SASM (Wu et al. 2012), could lead to an enhanced circulation (Hu et al. 2000).

101 However, the weakened thermal contrast in the upper troposphere might play a more

102 important role in a long-term trend and weakened SASM monsoon circulation (Sun et al.

103 2010). For the EASM, Jiang and Wang (2005) and Song et al. (2014) suggested that the

104 summer monsoon circulation over East Asia is slightly enhanced based on model

105 ensembles. It is further revealed that the increased GHG leads to enhanced western North

106 Pacific Subtropical High (WNPSH) and increased southerly on the western boundary of

107 WNPSH (Tian et al. 2018). Over ocean, Lee et al. (2008) suggested that the low-level

108 convergence decreases over the western North Pacific and the WNPSM weakens despite

109 of increasing moisture in the atmosphere in response to CO_2 increases.

110   Some anthropogenic aerosols (AA) can cause surface cooling by scattering and

111 absorbing solar radiation and change the radiative properties of clouds (Boucher et al. 2013).

112 Meanwhile, black carbon and organic carbon can absorb reflected solar radiation to increase

113 the atmospheric temperature (Menon et al. 2002; Ming et al. 2010; Ramanathan et al. 2001).

114 As AA emissions increased during the last few decades in Asia, it might affect the adjacent

115 precipitation by altering the land-sea thermal contrast and relative monsoon circulation (Ming

116 and Ramaswamy 2011; Rotstayn and Lohmann 2002; Dong et al. 2016). In SASM region,

117 the monsoon circulation changes in response to increased AA emissions are characterized

118 by an anomalous meridional overturning circulation that tends to decrease precipitation over

119 the Indian peninsula (Bollasina et al. 2011). Some model studies suggest the resulted

120 anomalous meridional SST gradient over the Indian Ocean with cooling on the North Indian

121 Ocean in response to AA emission changes is the main driver (Ganguly et al. 2012; Ganguly

122 et al. 2012; Ramanathan et al. 2005; Chung et al. 2006; Luo et al. 2019). In EASM region,

123 observations show a wet trend in south China and a drought trend in north in past several

124 decades and this pattern is considered as a result of increased aerosol emissions in China

125 (Wang 2001; Ding et al. 2008, 2009; Menon et al. 2002; Xie et al. 2016; Tian et al. 2018).

126 Some studies suggest that the aerosol can cause a regional cooling over land and leads to

127 a weakened land-sea thermal contrast and thus weakened EASM circulation and

128 precipitation (Ye et al. 2013; Song et al. 2014, Dong et al. 2016).

129   In Asian monsoon region, GHG and AA do not always play similar roles for the monsoon

130 decadal variations. Lau and Kim (2017) suggested that increases in GHG since 1950s

131 generate an increased land-sea thermal contrast but it is masked by the cooling induced by

132 AA forcing. This study also suggested that the EASM and SASM are having different

133 sensitivity to GHG and AA changes. In EASM region, as the circulation is weakened by AA

134 effect while GHG's role is negligible due to the offset by its dynamic effect and

135 thermodynamic effect, AA forcing is more dominating in the decreased monsoon circulation

136 and tends to reduce the precipitation (Zhang and Li 2016; Song et al. 2014). Luo et al. (2019)

137 suggested that reduction in precipitation in South Asia in last few decades is related to the

138 weakened SASM circulation in response to changes in both GHG and AA and that

139 circulation change induced precipitation decrease is stronger than the increase related to

140 moisture increase in the atmosphere. All above mentioned studies are on changes of GHG

141 and AA emissions on either the EASM or SASM. In contrast, the anthropogenic influences

142 on the SCSSM and physical processes involved are not fully investigated.

143   This study aims to elucidate the processes of how GHG and AA affect the inter-decadal

144 change of the SCSSM in the late 20th century, focusing on: 1) What is the role of

145 anthropogenic forcing to the observed inter-decadal change? 2) What are the relative roles

146 of changes in GHG and AA frocings? 3) What are the physical processes? We have

147 performed a set of model experiments using the atmospheric component of the state-of-the-

148 art HadGEM3 global climate model coupled to a multi-level mixed-layer ocean model to

149 address these questions.

150   Lots of studies about impacts of anthropogenic forcings on the EASM and SASM use

151 full ocean Coupled General Circulation Models (CGCM) including CMIP5 models (Song et

152 al. 2014; Seo et al. 2013; Chen et al. 2016; Sharmila et al. 2015), but these models usually

153 have significant bias on sea surface temperature (SST) in mean state (Li et al. 2012; 2015;

154 Levine et al. 2013). As the Australian-Asian monsoon is sensitive to SST, this bias may

155 cause even larger bias on monsoon simulation. Thus, MetUM-GOML models use an ocean

156 mixed-layer model replacing the 3D CGCMs, which can reduce the calculation cost and

157 have a smaller SST bias by a prescribed flux corrections (Hirons et al. 2015, Dong et al.

158 2017, Tian et al. 2018). So, this work will use a set of experiments based on the second

159 generation of GOML models (MetUM-GOML2).

160   The structure of this paper is as follows: Section 2 analyses the observational data and

161 describes the inter-decadal change of the SCSSM in the late 20th century. Section 3

162 introduces the model and detailed design of model experiments. Section 4 evaluates the

163 relative contributions of different forcings to the inter-decadal change. Sections 5 and 6

164 reveal the physical processes of changing GHG or AA forcing on the SCSSM respectively.

165 Finally, our conclusions are drawn in Section 7.

166

167 **2 Observed inter-decadal change**

168 In this study, we use monthly NOAA's Precipitation Reconstruction (PREC) dataset

169 (Chen et al. 2002) and precipitation based on GPCP (Adler et al. 2003). Observed 3D

170 monthly horizontal velocity and vertical velocity come from NCEP Reanalysis 1 (NCEP1;

171 Kalnay et al. 1996) while monthly sea level pressure (SLP) is obtained from Hadley Centre

172 Sea Level Pressure dataset (HadSLP2; Allan and Ansell 2006). All variables are averaged

173 from June to August to describe the boreal summer mean.

174 To show the inter-decadal variability (IDV) of rainfall change in observations, the area

175 averaged precipitation in the South China Sea region (10°N-20°N, 105°E-120°E) in JJA is

176 defined as an index and its time evolution is shown in Figure 1a. One of the most important

177 features of the time evolution of this precipitation index is the inter-decadal variation across

178 the 1990s, characterized by a positive precipitation anomaly from 1964 to 1981 (early period,

179 EP) and a negative precipitation anomaly from 1994 to 2011 (present day, PD). These

180 periods are selected also to avoid the impact of volcanic eruptions. The mean anomaly in

181 these two periods is 0.45 mm/day in EP and -0.14 mm/day in PD, respectively, which means

182 a -0.59 mm/day (which is about 13.6% of the climatological mean of 1979-2018 in GPCP

183 dataset) decrease from EP to PD.

184 We compare the spatial pattern of precipitation and circulation associated with this inter-

185 decadal change (PD minus EP) to understand the physical processes involved. It is found

186 that the inter-decadal decrease in precipitation mainly centered in the SCS (up to 0.5-2.0

187 mm/day), and was accompanied by anomalous anticyclonic circulation in the lower

188 troposphere (fig. 1b) with anomalous easterlies across the SCS. The anomalous easterlies

189 over the SCS indicate weakened climatological SCS westerlies in the summer from EP to

190 PD. The anomalous anticyclonic circulation is also associated with anomalous divergence

191 in the lower troposphere and anomalous convergence in the upper troposphere (Fig. 1c)

192 with anomalous descent in the whole troposphere (Fig. 1d), indicating weakened convection

193 in the SCS and therefore leading to reduced precipitation.

194 What had caused this inter-decadal decrease in precipitation and monsoon circulation

195 over the SCS seen in observations? To find out drivers and understand the dynamical

196 mechanisms behind it, we perform a set of time slice experiments with the atmospheric

197 component of the state-of-the-art HadGEM3 global climate model coupled to a multi-level

198 mixed-layer ocean model with changes in GHG and AA emissions together from EP to PD

199 or changes in GHG and AA forcing separately.

200

201 **3 Models and experiments**

202 **3.1 MetUM-GOML2 model and experiments settings**

203 In this work, MetUM-GOML2 (e.g., Hirons et al. 2015) is used to perform a set of

204 experiments. The atmospheric component of the MetUM-GOML2 is the Met Office Unified

205 Model (MetUM) at the fixed scientific configuration Global Atmosphere 6.0 (GA6.0) with N96

206 horizontal resolution (1.875° longitude and 1.25° latitude) and 85 vertical levels. A detailed

207 description of GA6.0 is given by Walters et al. (2017). The atmospheric model includes an

208 interactive tropospheric chemistry scheme (eight aerosol species are included: ammonium

209 sulphate, mineral dust, fossil fuel black carbon, fossil-fuel organic carbon, biomass-burning,

ammonium nitrate, sea-salt, and secondary organic aerosols from biogenic emissions. Both

aerosol-radiation interaction and aerosol-cloud interaction (including aerosol indirect effect

and semi-indirect effect) are considered. More details about the parameterization of aerosol

indirect effect are described by Jones et al. (2011) and Bellouin et al. (2011, 2013).

The oceanic component is a Multi-Column K Profile Parameterization mixed-layer ocean

model. The horizontal resolution of MC-KPP is the same as AGCM where they are coupled,

and below each AGCM grid point in ocean region is one water column. The atmospheric

and oceanic components are coupled every 3 hours. Since MC-KPP only simulate vertical

mixing in each grid point and exclude the ocean dynamics, the climatological seasonal

ocean 3D flux corrections are applied on ocean temperature and salinity (Large et al. 1994).

These corrections are intended to represent the mean advection in ocean and account for

biases in atmospheric surface fluxes.

The set of experiments used in this study is the same as those used to investigate SASM

decadal changes in Luo et al. (2019). Here, we use greenhouse gases (GHG) and

anthropogenic aerosol (AA) forcings averaged over 1994-2011 as PD conditions. For EP

forcing, GHG forcing is an average of 1964-1981 while AA forcing is an average of 1970-

1981. The details of experiments are summarized in Table 1. Firstly, a relaxation experiment

is run for 12 years (E0) forced by PD GHG and AA forcing. In this experiment, the MC-KPP

profiles of temperature and salinity were relaxed to a PD climatological ocean temperature

and salinity from the Met Office ocean analysis data (Smith and Murphy 2007). Then we

diagnosed the seasonal cycle of climatological daily-mean 3D ocean temperature and

salinity corrections from E0. These temperature and salinity are the same and are imposed

in all free running coupled experiments. Therefore, response in the model experiments to a

233 particular forcing change includes both the fast response to the forcing change (i.e. surface

234 and atmospheric process) and slow response mediated by forcing induced SST change.

235 For free coupled experiments, the EP experiment (EP) is forced by GHG and AA forcing of

236 EP while All forcing present day (PD-ALL) is forced by PD GHG and AA forcing. In addition,

237 two extra experiments, present-day GHG forcing (PD-GHG) with PD GHG but EP AA and

238 present-day AA forcing (PD-AA) with PD AA but EP GHG, that are used to analyze the

239 individual effect of GHG and AA. All coupled experiments are run for 60 years and only last

240 55 years of each experiment are used for analysis. In all experiments, the annual mean

241 concentrations of GHG are prescribed uniformly globally while the aerosol emissions include

242 seasonal cycle and spatial distribution. The spatial distribution of changes in annual mean

243 sulphur dioxide emissions between the two periods was illustrated in the Fig. 3 in Chen and

244 Dong (2019) where changes are characterized by decreases over North America and

245 Europe and increases over South Asia and East Asia.

246 The response of different forcing is estimated by the difference of climatology between

247 a pair of experiments. The difference of PD-ALL and EP represent the combine effect of

248 GHG and AA forcing difference, while PD-GHG minus EP and PD-AA minus EP are

249 estimation of individual effect of GHG forcing and AA forcing. The statistical significance of

250 the difference in a pair of models is assessed using a two tailed Student's t-test.

251

252 ### 3.2 Model climatology

253 In this section, some climatological features of PD experiment are compared with

254 observations. Fig.2a and b show the precipitation, SLP and 850hPa wind from June to

255 August (JJA) in PD-ALL forcing experiment and Fig.2c and d show the SLP and 850hPa

256   wind from NCEP reanalysis 1 and observed precipitation from Global Precipitation

257   Climatology Project (GPCP; Adler et al. 2003). In observations, spatial pattern of SLP is

258   characterized by low SLP over the Eurasia continent and high SLP on the tropical Indian

259   ocean and western North Pacific (WNP). This SLP distribution is associated with westerly

260   monsoon flow from India and it turns into southwesterly with cyclonic circulation over the

261   SCS, known as the monsoon trough. This westerly monsoon flow transports a large amount

262   of water vapor to the SCS and leads to moisture convergence there associated with the

263   cyclonic flow, inducing convection and producing large precipitation in the region.

264   The general features of summer climatological precipitation, low-level wind and land-

265   sea contract of SLP are well reproduced by GOML2 model. However, the westerly from the

266   Indian Ocean is stronger in the model due to the overestimated meridional land-sea SLP

267   contrast. Thus, the westerly wind and monsoon trough extend eastward into the WNP in the

268   model and the simulated precipitation in the monsoon trough is larger than in observations.

269   Despite these biases, the model simulates the summer climatological precipitation and

270   low-level circulation over East Asia and adjacent regions well compared with observations,

271   which suggests this model can be an appropriate tool to study the precipitation change over

272   the SCS in response to different forcings.

273

274   **4 Model simulated changes in response to different forcings**

275   To explore the effects of anthropogenic forcing on the SCSSM in model experiments,

276   the changes in precipitation, low-level circulation and 500hPa vertical velocity in response

277   to changes in both GHG and AA forcings are shown in Fig.3a. Model simulated responses

278   to changes in anthropogenic forcing from EP to PD are characterized by anomalous

easterlies from the WNP, across the SCS, into the Indian peninsula, indicating a weakening of climatological westerlies. The weakened westerlies are associated with reduced precipitation in latitude band of (10°N-20°N) and increased precipitation to the south. These features in the model simulations are similar to observed inter-decadal changes between PD and EP in observations (Fig.1b), indicating that the changes in anthropogenic forcing might have played a dominant role in the observed inter-decadal changes of the SCSSM and reduced precipitation over the SCS in the late 20th century.

Shown in Fig.3 b and c are model simulated changes in response to either changes in GHG or AA forcing. The patterns of large-scale circulation and precipitation in response to changes in AA forcing (Fig. 3c) are similar to changes in ALL forcing experiment (Fig. 3a). Although precipitation under GHG forcing reduces as well, the easterly anomaly over the SCS region is weak. These responses to individual forcing change indicate that model simulated weakening of the SCSSM and reduced precipitation over the SCS from EP to PD are predominantly due to changes in AA forcing (Fig.3a, c) with weak contributions from changes in GHG (Fig. 3b).

To investigate the processes that contribute to the precipitation changes in the model simulated responses to different forcings, the column integrated moisture flux transports and their convergences are shown in Fig.4. The moisture flux transports and their convergences are further decomposed into a dynamic component due to circulation change and a thermodynamic component due to humidity change (e.g., Li and Ting 2017, Tian et al. 2018).

In many aspects, the patterns of changes in moisture flux convergences and their magnitudes in response to different forcings (Fig. 4a, d, g) are similar to changes in model simulated precipitation responses (Fig. 3). This indicates that it is the moisture flux

302   convergence responsible for model simulated precipitation changes. However, changes in

303   dynamic components and thermodynamics components show some different features in

304   response to different forcings. In response to ALL forcing change, the dynamic components

305   (Fig.4b) show anomalous westward moisture flux transport and anomalous moisture

306   transport divergence from the WNP, across the SCS, into the SASM region. These

307   anomalies in dynamic components are partially offset by anomalous eastward moisture

308   transports and convergences due to thermodynamic components related to warming mainly

309   induced by changes in GHG (this will be discussed in section 5). In response to changes in

310   GHG forcing, the model simulated moisture convergence changes (Fig.4d) are weak over

311   the SCS due to compensation between the dynamic component related to weakened

312   circulation (Fig.4e) and thermodynamic component related to increased water vapor in the

313   atmosphere (Fig. 4f). In response to changes in AA forcing, the changes in moisture flux

314   transports and their divergences are predominantly due to dynamic components related to

315   circulation changes with weak contribution from changes in humidity (Fig. 4g, h, and i).

316   To quantify the regional precipitation changes over the SCS, area averaged precipitation

317   changes in observations and model simulated changes in response to different forcings are

318   shown in Figure 5a. ALL forcing change leads to a decrease in precipitation by 0.32mm/day

319   and contributes approximately 72% of observed inter-decadal decrease (-0.44mm/day),

320   suggesting anthropogenic forcing changes from EP to PD might have been a dominating

321   effect for observed inter-decadal decrease in precipitation in the late 20th century. Individual

322   forcing both have a positive contribution on precipitation decrease with a dominant

323   contribution from changes in AA forcings. The regional averaged moisture transport

324   convergence is shown in Figure 5c. As the total moisture transport convergence shows a

similar change as precipitation in Fig.5a, the dynamic and thermodynamic components

clearly show how anthropologic forcings change circulation and humidity, and contribute to

the interdecadal deceased precipitation. All forcing, GHG forcing and AA forcing result in

weakened dynamic moisture transport convergence. However, as GHG changes warm the

atmosphere significantly, the thermodynamic part of all forcing and GHG forcing increases

and this offsets the dynamic component partially. AA emission changes do not change the

humidity much, so the thermodynamic component in AA forcing is weak and the weakened

total moisture transport convergence is predominantly related to changes in circulation. It

should be noted a nonlinearity of changes in the SCSSM in response to changes in GHG

and AA emissions (i.e., the response to the combined forcings is not necessarily equal to

the sum of the responses to the individual forcings). In particular, the sum of precipitation

changes over the SCS in response to GHG and AA changes is larger than the change in

response to ALL forcing. The nonlinearity noticed in this study is consistent with some

previous studies (Feichter et al. 2004, Ming and Ramaswamy 2009, Shiogama et al. 2012).

However, detailed investigation of the causes in this nonlinearity is beyond the scope of this

study.

The regional averaged zonal wind components over southern SCS (5°N-15°N, 105°E-

120°E) are shown in Fig.5b. In observations and model experiments, zonal wind in this

region change most significantly. This figure further illustrates that the weakened

precipitation over the SCS in response to changes in anthropogenic forcing (ALL forcing) is

mainly contributed by the weakened zonal wind and reduced moisture transports, and the

response to AA forcing plays a dominant role. In summary, it has demonstrated that the

circulation and precipitation changes in response to changes in individual GHG or AA forcing

348   show different characteristics. Thus, in the next two sections, we are exploring physical

349   processes that are responsible for the large-scale circulation differences in response to

350   individual forcing respectively.

351

352   **5 Mechanism related to GHG forcing**

353   The model simulated precipitation changes under GHG forcing show some weak

354   decreases, mainly resulted from the moisture flux transport compensation between the

355   dynamic component related to weakened circulation and thermodynamic component related

356   to increased humidity.   What processes are responsible for the circulation and humidity

357   changes in the model simulations?

358   In GHG forcing experiment, large scale anomalous descends cover a large area

359   including the SASM region and the SCS region, accompanied by a low-level easterly

360   anomaly (Fig.3b). These anomalous local circulation anomalies and descents are

361   associated with anomalous large-scale divergent circulations in the tropical Indian and

362   Pacific oceans (Fig. 6). These anomalous large-scale circulations indicate anomalous

363   convergence over the tropical eastern Pacific in the lower troposphere and anomalous

364   divergence in the upper troposphere with opposite changes over the tropical Indian ocean

365   and the western tropical Pacific, being associated with weakened Walker circulation.

366   Associated with these large-scale divergent circulations are that SST warming is stronger in

367   the eastern tropical Pacific (over 0.5℃) than western tropical Pacific (about 0.3℃) (Fig.7b),

368   indicating a weakening zonal SST gradient in the tropical Pacific. This association between

369   the change in zonal SST gradient and large scale divergent circulations is consistent with

370   previous researches which suggested that the zonal SSTA gradient change associated with

371   El-Nino like SST anomalies enhances convection over the eastern equatorial Pacific and

372   leads to a weakened Walker circulation over the tropics (Ju and Slingo 1995; Timmermann

373   et al. 1999; Wilhelm, 2002).

374   How do changes in GHG forcing lead to enhanced warming over the eastern tropical

375   Pacific than in western tropical Pacific?   Firstly, GHG forcing changes surface radiation

376   balance. With increase in GHG forcing, both clear sky surface longwave radiation (clear-sky

377   LW) and surface longwave cloud radiative effect (CRE-LW) increase over the equatorial

378   Pacific (Fig.7c and 7d). Because mixed layer depth is deeper in the western tropical Pacific

379   than in the eastern tropical Pacific, the response of SSTA is weaker in the west and stronger

380   in the east. This zonal asymmetry leads to a weakened zonal SST gradient and Walker

381   circulation through the dynamic processes elucidated above. This mechanism agrees with

382   previous research (DiNezio et al. 2009; Yeh et al. 2009; Collins et al. 2010) which revealed

383   the relationship of climate change, El-Nino like SSTA change and relative trade wind change.

384   Secondly, as air temperature increases due to increasing GHG concentrations, atmosphere

385   can hold more moisture over the SCS. Warmer sea surface temperature can also increase

386   the evaporation locally so both these changes lead to increase in the water vapor in the

387   atmosphere (Fig.7a).

388   The results above indicate that the decreasing precipitation and weakened monsoon

389   circulation over the SCS in GHG forcing experiments are caused by anomalous descend

390   which is related to weakened Walker circulation.

391

392   **6 Mechanism related to AA forcing**

393   In response to changes in AA forcing, the changes in moisture flux transports and their

394 divergences are predominantly due to dynamic components related to circulation changes

395 with weak contribution from changes in humidity (Fig. 4g, h, i). In AA forcing experiment,

396 there are significant easterly anomalies over the monsoon region from the Arabian Sea to

397 the western North Pacific (Fig. 3c).

398   To understand the mechanism of these circulation changes, we analyze the zonal mean

399 (60°E-150°E) meridional overturning circulation changes in response to AA forcing (Fig.8a).

400 These anomalous overturning circulations are characterized by anomalous descents around

401 monsoon region (10°N-25°N) and anomalous ascends around the equator, indicating a

402 change in local Hadley circulation. Previous researches suggest that this anomalous local

403 Hadley circulation might be a result of SSTA meridional gradient (Ganguly et al. 2012;

404 Ganguly et al. 2012; Ramanathan et al. 2005; Chung et al. 2006; Luo et al. 2019). However,

405 the SSTA gradient change in JJA is weak in response to AA forcing (Fig. 8b). The SSTA

406 over ascend region is about -0.05℃ and it is about 0℃ over descend region (Fig8b). This

407 association between anomalous ascents (descents) with anomalous cold (weak) SST

408 seems counterintuitive. However, this simultaneous association includes atmospheric

409 feedbacks on SST changes. Thus, we explore the SSTA in pre-monsoon seasons (Fig.9).

410 There is no significant SSTA over the northern Indian Ocean (NIO) and the SCS in JJA, but

411 during December to February (DJF) and March to May (MAM), SST is cooled to the north

412 of the equator in this region (about -0.1℃ to -0.3℃). This meridional SST gradient in pre-

413 monsoon seasons is key processes for local Hadley circulation anomaly in JJA.

414   To understand the process of how aerosol changes affect SSTA and circulation in the

415 pre-monsoon seasons, seasonal evolutions of zonal averaged changes over the monsoon

416 region (60°E-150°E) are analyzed and they are illustrated in Fig. 10. Results indicate that

large summer monsoon precipitation and circulation changes occur in June and become

weaker in July and August (Fig.10a and 10b). The meridional SSTA gradient with relative

large cold anomalies of about 0.2℃ in the northern subtropics sustains during pre-monsoon

seasons until it gets weaker after May and June when monsoon establishes (Fig.10c). This

SSTA pattern and associated meridional SST gradient (cooler in north than in south)

sustains until May and June when it drives a local Hadley circulation which causes an

anomalous descend over monsoon region and then weakened westerly low-level flow and

less precipitation.

This SSTA annual cycle is driven by surface radiation changes. In response to AA

forcing, clear-sky surface shortwave radiation (clear-sky SW) decreases all year round over

the ocean with maximum changes during SON and MAM (Fig.10d), which cause a cooler

SSTA locally. The clear-sky SW changes are closely related to the aerosol-radiation

interaction and aerosol-cloud interaction. Changes in aerosol optical depth (AOD), cloud

droplet effective radius (CDER) and cloud droplet number (CDN) are larger over the NIO

and the SCS in pre-monsoon seasons (largest during SON) than in JJA since aerosol

emissions are advected by the prevailing winds to these regions (Fig.11j-11i). These

changes are characterized by increases in AOD, decreases in CDER, and increases in CDN.

Note that seasonal changes in CDER show some differences in comparison with changes

in AOD and CDN since CDER-CDN relationship is not linear (Jones et al. 2001) and CDER

change is more sensitive to the basic state environment than CDN over ocean where the

atmosphere is cleaner (Carslaw et al. 2013). These changes in AOD, CDN, and CDER are

responsible for the seasonal evolutions of changes in surface clear sky SW and SST (Fig.

10c, d).   As a result, the SSTA is cool over the NIO to equatorial IO since SON and sustains

440   until May and Jun.

441   In May and June, the SST is still cooler over the NIO than around the equator, which

442   drives a local Hadley circulation. However, upward surface latent heat flux reduces related

443   to weakened low-level westerlies (anomalous easterlies) over monsoon region (positive

444   downward in Fig.10e). Meanwhile shortwave cloud radiative effect shows positive changes

445   (CRE-SW, Fig.10f) due to less cloud cover associated with reduced convection. These

446   feedbacks associated with the changes in circulation and surface radiation damp cold SST

447   anomalies induced by AA change in pre-monsoon seasons, leading to weak SST anomalies

448   in JJA and weak meridional SST gradient.

449   In summary, when changes in AA emissions are advected by prevailing winds from the

450   Asian continent to the NIO and the SCS in pre-monsoon seasons, the SST is cooled by

451   reduced clear sky SW while changes in both clear sky SW radiation and SST are weak in

452   the southern hemisphere. These result in anomalous meridional SST gradient in Asian

453   sector and this meridional SST gradient sustains until boreal summer, which in turn drives

454   weakened monsoon circulation and precipitation over the SCS in summer. In May and June

455   when precipitation is reduced, the SST warms over the NIO due to increased shortwave

456   cloud radiative effect (Fig. 10f) related to reduced cloud cover and weakened latent heat flux

457   (Fig. 10e) related to weakened westerlies. These processes tend to damp cold SST

458   anomalies in pre-monsoon seasons lead to weak summer mean SST anomalies over the

459   NIO (Fig.9d, Fig. 10c).

460

461   **7 Conclusion and discussion**

462   Base on observations, there is a significant inter-decadal decrease of precipitation over

463   the SCS between 1964-1981 and 1994-2011 during boreal summer monsoon season (JJA).

464   Corresponding to the change in precipitation is a weakened SCSSM circulation,

465   characterized by anomalous descend over the SCS, weaker westerly monsoon flow in the

466   lower troposphere and less moisture flux transport convergence to the SCSSM region. In

467   this study, a set of experiments based on MetUM-GOML2 model is used to investigate the

468   role of anthropogenic forcing (including GHG and AA emission) changes and quantify the

469   relative roles of GHG and AA forcing, on the inter-decadal decrease of the SCSSM and

470   precipitation.   The main results are summarized as follows:

471   1.   Model results suggest that the changes in anthropogenic forcing from EP (1964-

472   1981) to PD (1994-2011) might have played a dominant role in the observed inter-decadal

473   changes of the SCSSM and reduced precipitation in the late 20th century in which AA forcing

474   plays a more important role compared with GHG forcing.

475   2.   Increased GHG concentrations lead to positive changes in surface longwave

476   radiation over the tropical Pacific. Due to the asymmetric mixed layer depth, warming in the

477   eastern equatorial Pacific is greater than in the western tropical Pacific. This El-Niño-like

478   SSTA pattern leads to a weaker Walker circulation and causes a large-scale descend in

479   both Indian monsoon and SCS monsoon region, and causes a weaker westerly low-level

480   flow. This weakened monsoon circulation leads to weakened moisture flux transport

481   convergence and therefore reduced precipitation over the SCS. Meanwhile, the warm SST

482   anomalies lead to increases of evaporation and the water vapor in the atmosphere. This

483   leads to increased moisture flux transport convergence and therefore enhanced

484   precipitation over the SCS. Due to this compensation between dynamical moisture transport

485   and thermodynamic moisture transport, the changes in moisture transport convergence, and

486 therefore precipitation over the SCS are weak.

487 3.   In response to changes in AA emissions, CDN and AOD increase while CDN

488 decreases over continental Asia due to increased AA emissions over Asia. In pre-monsoon

489 seasons, aerosol emissions are transported to the northern Indian Ocean and the SCS by

490 prevailing winds, leading to increases in CDN and AOD and decreases in CDER in these

491 regions. These changes lead to reduced surface clear-sky shortwave radiation in the

492 northern subtropics with weak changes in southern hemisphere. As a result, the SST in the

493 northern subtropics decreases by about $0.2°C$ in pre-monsoon seasons and this cold

494 anomaly sustains until the establishment of summer monsoon. This nonuniform SST change

495 leads to a meridional SST gradient which in turn induces a local Hadley circulation change

496 with anomalous descending at monsoon region and the anomalous easterly wind in the

497 lower troposphere which transport less moisture to the SCS monsoon region, leading to

498 reduced precipitation.

499 Our modelling results suggest that changes in GHG concentrations and AA emissions

500 might have played an important role in decreased SCSSM and reduced precipitation on the

501 SCS in the late 20th century in which AA forcing plays a more important role compared with

502 GHG forcing. This result is in agreement to some previous researches about role of AA

503 changes in the East Asian summer monsoon based on CMIP5 models (Song et al. 2014;

504 Zhang and Li 2016) .

505 Although the observed inter-decadal decrease of SCSSM precipitation can be captured

506 by this model, it should be pointed out that these results and processes are based on this

507 specific model and experiment design. For example, these experiments use GHG and AA

508 forcing of two specific periods (1964-1981 and 1994-2011) and the ocean model is a mixed

509 layer model. Therefore, the role of ocean dynamics are not included in our experiments. In

510 the future, the reliability of the physical processes in this study can be tested by comparing

511 with other models' results which consider the oceanic circulation changes in response to

512 different forcings. In addition, it should be noted a nonlinearity of changes in the SCSSM in

513 response to changes in GHG and AA emissions (i.e., the response to the combined forcings

514 is not necessarily equal to the sum of the responses to the individual forcings). The

515 nonlinearity noticed in this study is consistent with some previous studies (Feichter et al.

516 2004, Ming and Ramaswamy 2009, Shiogama et al. 2012), and needs to be investigated

517 further.

518

527

528
529

530 Reference:

531 Adler RF, Huffman GJ, Chang A, et al (2003) The Version-2 Global Precipitation Climatology

532   Project (GPCP) Monthly Precipitation Analysis (1979–Present). J Hydrometeorol. doi:

533   10.1175/1525-7541(2003)004<1147:tvgpcp>2.0.co;2

534 Allan R, Ansell T (2006) A new globally complete monthly historical gridded mean sea level

535   pressure dataset (HadSLP2): 1850-2004. J Clim. doi: 10.1175/JCLI3937.1

536 Bellouin N, Mann GW, Woodhouse MT, et al (2013) Impact of the modal aerosol scheme

537   GLOMAP-mode on aerosol forcing in the hadley centre global environmental model.

538   Atmos Chem Phys. doi: 10.5194/acp-13-3027-2013

539 Bellouin N, Rae J, Jones A, et al (2011) Aerosol forcing in the Climate Model

540   Intercomparison Project (CMIP5) simulations by HadGEM2-ES and the role of

541   ammonium nitrate. J Geophys Res Atmos. doi: 10.1029/2011JD016074

542 Bollasina MA, Ming Y, Ramaswamy V (2011) Anthropogenic Aerosols and the Summer

543   Monsoon. Science (80-) 334:502–505

544 Boucher O, Randall D, Artaxo P, Bretherton C, Feingold G, Forster P, Zhang X (2013)

545   Clouds and aerosols. In: Stocker T et al (eds) Climate change 2013: the physical

546   science basis. Contribution of working group I to the fifth assessment report of the

547   intergovernmental panel on climate change. Cambridge University Press, Cambridge,

548   pp 571–657

549 Carslaw KS, Lee LA, Reddington CL, Pringle KJ, Rap A, Forster PM, Mann GW, Spracklen

550   DV, Woodhouse MT, Regayre LA, Pierce JR (2013) Large contribution of natural

551   aerosols to uncertainty in indirect forcing. Nature 503:67–71

552 Charlson RJ, Schwartz SE, Hales JM, et al (1992) Climate forcing by anthropogenic

553   aerosols. Science (80-). doi: 10.1126/science.255.5043.423

554 Chen L and O. W. Frauenfeld (2016) A comprehensive evaluation of precipitation

555   simulations over China based on CMIP5 multimodel ensemble projections. J Geophys

556   Res Atmos 121:5430–5452. doi: 10.1002/2013JD021190.Received

557 Chen M, Xie P, Janowiak JE, Arkin PA (2002) Global Land Precipitation: A 50-yr Monthly
558   Analysis Based on Gauge Observations. J Hydrometeorol. doi: 10.1175/1525-
559   7541(2002)003<0249:glpaym>2.0.co;2

560 Chen W, and Dong B (2019) Anthropogenic impacts on recent decadal change in
561   temperature extremes over China: Relative roles of greenhouse gases and
562   anthropogenic aerosols. *Climate Dyn.* 52, 3643–3660, doi: 10.1007/s00382-018-4342-
563   9.

564 Chung CE, Ramanathan V (2006) Weakening of north Indian SST gradients and the
565   monsoon rainfall in India and the Sahel. J Clim. doi: 10.1175/JCLI3820.1

566 Collins M, An S II, Cai W, et al (2010) The impact of global warming on the tropical Pacific
567   Ocean and El Nĭo. Nat Geosci 3:391–397. doi: 10.1038/ngeo868

568 Dai N, Xie A, Zhang Y (2000) Interannual and Interdecadal Variations of Summer Monsoon
569   Activities over South China Sea[J]. Climatic and Environmental Research(in
570   Chinese),5(4):363-374,doi:10.3878/j.issn.1006-9585.2000.04.04.

571 Ding Y (1992) Summer monsoon rainfall in China. J. Meteorol. Soc. Jpn. 70, 373–396

572 Ding Y, Sun Y, Wang Z, et al (2009) Inter-decadal variation of the summer precipitation in
573   China and its association with decreasing Asian summer monsoon Part II: Possible
574   causes. Int J Climatol 29:1926–1944. doi: 10.1002/joc.1759

575 Ding Y, Wang Z, Sun Y (2008) Inter-decadal variation of the summer precipitation in East
576   China and its association with decreasing Asian summer monsoon. Part I: Observed
577   evidences. Int J Climatol. doi: 10.1002/joc.1615

578 DiNezio PN, Clement AC, Vecchi GA, et al (2009) Climate response of the equatorial pacific
579   to global warming. J Clim 22:4873–4892. doi: 10.1175/2009JCLI2982.1

580 Dong B, Gregory JM, Sutton RT (2009) Undestanding land-sea warming contrast in
581   response to increasing greenhouse gases. Part I: Transient adjustment. J Clim

582   22:3079–3097. doi: 10.1175/2009JCLI2652.1

583   Dong B, Sutton RT, Highwood EJ, Wilcox LJ (2016) Preferred response of the East Asian
584   summer monsoon to local and non-local anthropogenic sulphur dioxide emissions. Clim
585   Dyn 46:1733–1751. doi: 10.1007/s00382-015-2671-5

586   Feichter J, Roeckner E, Lohmann U, Liepert B (2004) Nonlinear aspects of the climate
587   response to greenhouse gas and aerosol forcing. J Clim 17:2384–2398

588   Ganguly D, Rasch PJ, Wang H, Yoon JH (2012a) Fast and slow responses of the South
589   Asian monsoon system to anthropogenic aerosols. Geophys Res Lett 39:1–5. doi:
590   10.1029/2012GL053043

591   Ganguly D, Rasch PJ, Wang H, Yoon JH (2012b) Climate response of the South Asian
592   monsoon system to anthropogenic aerosols. J Geophys Res Atmos 117:1–20. doi:
593   10.1029/2012JD017508

594   Goswami B, Madhusoodanan M, Neema C, Sengupta D (2006) A physical mechanism for
595   North Atlantic SST influence on the Indian summer monsoon. Geophys Res Lett 33,
596   L02706. doi: 10.1029/2005GL024803

597   Guo L, Highwood EJ, Shaffrey LC, Turner AG (2013) The effect of regional changes in
598   anthropogenic aerosols on rainfall of the East Asian Summer Monsoon. Atmos Chem
599   Phys. doi: 10.5194/acp-13-1521-2013

600   Held IM, Soden BJ (2006) Robust responses of the hydrologic cycle to global warming. J
601   Clim. doi: 10.1175/JCLI3990.1

602   Hu ZZ, Latif M, Roeckner E, Bengtsson L (2000) Intensified Asian summer monsoon and its
603   variability in a coupled model forced by increasing greenhouse gas concentrations.
604   Geophys Res Lett 27:2681–2684. doi: 10.1029/2000GL011550

605   JIANG D and Wang H (2005) Natural interdecadal weakening of East Asian summer
606   monsoon in the late 20th century. Chinese Sci Bull 50:1923. doi: 10.1360/982005-36

607   Jones A, Roberts DL, Woodage MJ, Johnson CE (2001) Indirect sulphate aerosol forcing in

a climate model with an interactive sulphur cycle. J Geophys Res 106 D17: 20,293–20,310

Jones CD, Hughes JK, Bellouin N, et al (2011) The HadGEM2-ES implementation of CMIP5 centennial simulations. Geosci Model Dev. doi: 10.5194/gmd-4-543-2011

Ju J, Slingo J (1995) The Asian summer monsoon and ENSO. Q J R Meteorol Soc. doi: 10.1002/qj.49712152509

Kalnay E, Kanamitsu M, Kistler R, et al (1996) The NCEP/NCAR 40-year reanalysis project. Bull Am Meteorol Soc. doi: 10.1175/1520-0477(1996)077<0437:TNYRP>2.0.CO;2

Lamarque JF, Bond TC, Eyring V, et al (2010) Historical (1850-2000) gridded anthropogenic and biomass burning emissions of reactive gases and aerosols: Methodology and application. Atmos Chem Phys. doi: 10.5194/acp-10-7017-2010

Lau NC, Ann MJ, Wang H (2005). Simulations by a GFDL GCM of ENSO-related variability of the coupled atmosphere-ocean system in the East Asian Monsoon region. East Asian Monsoon.

Lau NC., Wang B. (2006) Interactions between the Asian monsoon and the El Niño/Southern Oscillation. In: The Asian Monsoon. Springer Praxis Books. Springer, Berlin, Heidelberg

Lau KM, Kim KM (2017) Competing influences of greenhouse warming and aerosols on Asian summer monsoon circulation and rainfall. Asia-Pacific J Atmos Sci 53:181–194. doi: 10.1007/s13143-017-0033-4

Lau KM, Yang S (1997) Climatology and interannual variability of the Southeast Asian summer monsoon. Adv Atmos Sci. doi: 10.1007/s00376-997-0016-y

Lee SM, Jhun JG, Kwon M, Kim W (2008) Change in the western North Pacific summer monsoon circulation due to the CO_2 increase in IPCC AR4 CGCMs. Asia Pac J Atmos Sci 44(4):351–368

Levine RC, Turner AG, Marathayil D, Martin GM (2013) The role of northern Arabian Sea surface temperature biases in CMIP5 model simulations and future projections of Indian

634   summer monsoon rainfall. Clim Dyn 41:155–172. doi: 10.1007/s00382-012-1656-x

635   Li C, and Zhang L, (1999) Summer monsoon activities in the South China Sea and its
636   impacts. Chin. J. Atmos. Sci., 23, 257–266.

637   Li G, Xie SP (2012) Origins of tropical-wide SST biases in CMIP multi-model ensembles.
638   Geophys Res Lett 39:1–5. doi: 10.1029/2012GL053777

639   Li G, Xie SP, Du Y (2015) Monsoon-induced biases of climate models over the tropical
640   Indian Ocean. J Clim 28:3058–3072. doi: 10.1175/JCLI-D-14-00740.1

641   Li J, Wu Z, Jiang Z, He J (2010) Can global warming strengthen the East Asian summer
642   monsoon? J Clim. doi: 10.1175/2010JCLI3434.1

643   Li X, Ting M (2017) Understanding the Asian summer monsoon response to greenhouse
644   warming: the relative roles of direct radiative forcing and sea surface temperature
645   change. Clim Dyn. doi: 10.1007/s00382-016-3470-3

646   Li X, Ting M, Li C, Henderson N (2015) Mechanisms of Asian Summer Monsoon Changes
647   in Response to Anthropogenic Forcing in CMIP5 Models*. J Clim. doi: 10.1175/jcli-d-
648   14-00559.1

649   Li Z, Lau WKM, Ramanathan V, et al (2016) Aerosol and monsoon climate interactions over
650   Asia. Rev. Geophys.

651   Liang J, Wu S, and You J, (1999) The research on variations of onset time of the SCS
652   summer monsoon and its intensity. Chin. J. Trop. Meteor., 15, 97–105.

653   Lu E. and Chan J, (1999) A Unified Monsoon Index for South China. J. Climate, 12, 2375–
654   2385, doi: 10.1175/1520-0442(1999)012<2375:AUMIFS>2.0.CO;2

655   Lu R, Dong B, Ding H (2006) Impact of the Atlantic Multidecadal Oscillation on the Asian
656   summer monsoon. Geophys Res Lett 33:1–5. doi: 10.1029/2006GL027655

657   Luo F, Dong B, Tian F, Li S (2019) Anthropogenically Forced Decadal Change of South
658   Asian Summer Monsoon Across the Mid-1990s. J Geophys Res Atmos 124:806–824.
659   doi: 10.1029/2018JD029195

660 Murakami T., Matsumoto J. (1994). Summer monsoon over the Asian continent and western

661   north Pacific. J. Meteorol. Soc. Jpn. 72, 719–745.

662 May W (2002) Simulated changes of the Indian summer monsoon under enhanced

663   greenhouse gas conditions in a global time-slice experiment. Geophys Res Lett. doi:

664   10.1029/2001GL013808

665 Menon S, Hansen J, Nazarenko L (2002) Climate Effects of Black Carbon Aerosols in China

666   and India. 297:2250–2254

667 Ming Y, Ramaswamy V (2009) Nonlinear climate and hydrological responses to aerosol

668   effects. J Clim 22:1329–1339

669 Ming Y, Ramaswamy V, Persad G (2010) Two opposing effects of absorbing aerosols on

670   global-mean precipitation. Geophys Res Lett 37:1–4. doi: 10.1029/2010GL042895

671 Ming Y, Ramaswamy V (2011) A model investigation of Aerosol-Induced changes in tropical

672   circulation. J Clim. doi: 10.1175/2011JCLI4108.1

673 Pitari G, Ackerman A, Adams P, et al (2001) Aerosols, their Direct and Indirect Effects. Clim

674   Chang 2001 Sci Basis Contrib Work Gr I to Third Assess Rep Intergov Panel Clim

675   Chang 5:289–348

676 Prell WL (2011) Variation of monsoonal upwelling: A response to changing solar radiation

677 Ramanathan V, Chung C, Kim D, et al (2005) Atmospheric brown clouds: Impacts on South

678   Asian climate and hydrological cycle. Proc Natl Acad Sci. doi:

679   10.1073/pnas.0500656102

680 Ramanathan V, Crutzen PJ, Kiehl JT, Rosenfeld D (2001) Atmosphere: Aerosols, climate,

681   and the hydrological cycle. Science (80-) 294:2119 – 2124. doi:

682   10.1126/science.1064034

683 Rotstayn LD, Lohmann U (2002) Tropical rainfall trends and the indirect aerosol effect. J

684   Clim. doi: 10.1175/1520-0442(2002)015<2103:TRTATI>2.0.CO;2

685 Seo KH, Ok J, Son JH, Cha DH (2013) Assessing future changes in the East Asian summer

686   monsoon using CMIP5 coupled models. J Clim 26:7662–7675. doi: 10.1175/JCLI-D-12-
687   00694.1

688   Sharmila S, Joseph S, Sahai AK, et al (2015) Future projection of Indian summer monsoon
689   variability under climate change scenario: An assessment from CMIP5 climate models.
690   Glob Planet Change 124:62–78. doi: 10.1016/j.gloplacha.2014.11.004

691   Shiogama H, Stone DA, Nagashima T, Nozawa T, Emori S (2012) On the linear additivity of
692   climate forcing-response relationships at global and continental scales Int. J Climatol
693   33:2542–2550

694   Smith DM, Murphy JM (2007) An objective ocean temperature and salinity analysis using
695   covariances from a global climate model. J Geophys Res Ocean. doi:
696   10.1029/2005JC003172

697   Song F, Zhou T, Qian Y (2014) Responses of East Asian summer monsoon to natural and
698   anthropogenic forcings in the 17 latest CMIP5 models. Geophys Res Lett. doi:
699   10.1002/2013GL058705

700   Sun Y, Ding Y, Dai A (2010) Changing links between South Asian summer monsoon
701   circulation and tropospheric land-sea thermal contrasts under a warming scenario.
702   Geophys Res Lett 37:1–5. doi: 10.1029/2009GL041662

703   Sutton RT, Dong B, Gregory JM (2007) Land/sea warming ratio in response to climate
704   change: IPCC AR4 model results and comparison with observations. Geophys Res Lett
705   34:2–6. doi: 10.1029/2006GL028164

706   Tanaka HL, Ishizaki N, Kitoh A (2004) Trend and interannual variability of Walker, monsoon
707   and Hadley circulations defined by velocity potential in the upper troposphere. Tellus,
708   Ser A Dyn Meteorol Oceanogr 56:250–269. doi: 10.1111/j.1600-0870.2004.00049.x

709   Tao S, Chen L. (1987) A review of recent research on the East Asian summer monsoon in
710   China. In:Chang,C.-P.,Krishnamurti, T.N. (Eds.), Monsoon Meteorology. Oxford
711   University Press, New York, pp. 60–92.

712 Tian F, Dong B, Robson J, Sutton R (2018) Forced decadal changes in the East Asian

713   summer monsoon: the roles of greenhouse gases and anthropogenic aerosols. Clim

714   Dyn 51:3699–3715. doi: 10.1007/s00382-018-4105-7

715 Timmermann A, Oberhuber J, Bacher A, et al (1999) Increased El Nino frequency in a

716   climate model forced by future greenhouse warming. Nature. doi: 10.1038/19505

717 Tong HW, Chan JCL, Zhou W (2009) The role of MJO and mid-latitude fronts in the South

718   China Sea summer monsoon onset. Clim Dyn 33:827–841. doi: 10.1007/s00382-008-

719   0490-7

720 Trenberth KE, Shea DJ (2006) Atlantic hurricanes and natural variability in 2005. Geophys

721   Res Lett 33:1–4. doi: 10.1029/2006GL026894

722 Ueda H, Iwai A, Kuwako K, Hori ME (2006) Impact of anthropogenic forcing on the Asian

723   summer monsoon as simulated by eight GCMs. Geophys Res Lett 33:20–23. doi:

724   10.1029/2005GL025336

725 Vecchi GA, Soden BJ (2007) Global warming and the weakening of the tropical circulation.

726   J Clim. doi: 10.1175/JCLI4258.1

727 Walters D, Boutle I, Brooks M, et al (2017) The Met Office Unified Model Global Atmosphere

728   6.0/6.1 and JULES Global Land 6.0/6.1 configurations. Geosci Model Dev. doi:

729   10.5194/gmd-10-1487-2017

730 Wang B, Huang F, Wu Z, et al (2009) Multi-scale climate variability of the South China Sea

731   monsoon: A review. Dyn. Atmos. Ocean.

732 Wang Z. & Qian Y. (2009) The relationship of land-ocean thermal anomaly difference with

733   mei-yu and South China Sea summer monsoon Adv. Atmos. Sci. 26: 169. doi:

734   10.1007/s00376-009-0169-y

735 Wang B, Yim SY, Lee JY, et al (2014) Future change of Asian-Australian monsoon under

736   RCP 4.5 anthropogenic warming scenario. Clim Dyn. doi: 10.1007/s00382-013-1769-x

737 Wang B, Zhang Q (2002) Pacific-East Asian teleconnection. Part II: How the Philippine Sea

738   anomalous anticyclone is established during El Niño development. J Clim. doi:
739   10.1175/1520-0442(2002)015<3252:PEATPI>2.0.CO;2

740 Wang C (2004) A modeling study on the climate impacts of black carbon aerosols. J
741   Geophys Res Atmos. doi: 10.1029/2003jd004084

742 Wen Z, Huang R, He H, and Lan G (2006) The influences of anomalous atmospheric
743   circulation over mid-high latitudes and the activities of 30-60d low frequency convection
744   over low latitudes on the onset of the South China Sea summer monsoon. Chin. J.
745   Atmos. Sci., 30, 952–964.

746 Wu G, Liu Y, He B, et al (2012) Thermal controls on the asian summer monsoon. Sci Rep
747   2:1–7. doi: 10.1038/srep00404

748 Wu S, and Liang J (2001) An index of South China Sea summer monsoon intensity and its
749   characters. Chin. J. Trop. Meteor., 17, 337–344.

750 Xie X, Wang H, Liu X, et al (2016), Distinct effects of anthropogenic aerosols on the East
751   Asian summer monsoon between multidecadal strong and weak monsoon stages, J.
752   Geophys. Res. Atmos., 121, 7026– 7040, doi:10.1002/2015JD024228.

753 Yao Y, and Qian Y (2001) A study on the South China Sea monsoon index and the
754   relationship between the index and regional rainfalls of China. J. Nanjing Uni., 37, 781–
755   788

756 Ye J, Li W, Li L, Zhang F (2013) "North drying and south wetting" summer precipitation
757   trend over China and its potential linkage with aerosol loading. Atmos Res 125–126:12–
758   19. doi: 10.1016/j.atmosres.2013.01.007

759 Yeh SW, Kug JS, Dewitte B, et al (2009) El Nĩo in a changing climate. Nature 461:511–514.
760   doi: 10.1038/nature08316

761 Zhang L, Li T (2016) Relative roles of anthropogenic aerosols and greenhouse gases in land
762   and oceanic monsoon changes during past 156 years in CMIP5 models. Geophys Res
763   Lett. doi: 10.1002/2016GL069282

764 Zhou T, Gong D, Li J, Li B (2009) Detecting and understanding the multi-decadal variability
765   of the East Asian Summer Monsoon – Recent progress and state of affairs, Meteorol.
766   Z., 18, 455–467.

767 Zhou W, Chan JCL (2005) Intraseasonal oscillations and the South China Sea summer
768   monsoon onset. Int J Climatol 25:1585–1609. doi: 10.1002/joc.1209

769 Zhou W, Chan JCL. ENSO and the South China Sea summer monsoon onset[J].
770   International Journal of Climatology, 2010, 27(2):157-167. doi：10.1002/joc.1380

771 Zhu Y, Wang H, Zhou W, Ma J (2011) Recent changes in the summer precipitation pattern
772   in East China and the background circulation. Clim Dyn 36:1463 – 1473. doi:
773   10.1007/s00382-010-0852-9

774   Table 1 Summarize of numerical experiments

775

Experiment		Ocean	Radiative Forcing
E0	Relaxation run	Relax to PD mean 3D ocean temperature and salinity to diagnose climatological temperature and salinity flux correction	Climatological PD (1994-2011) greenhouse gases (GHG) and anthropogenic aerosol (AA) precursor emissions. The GHG and AA forcing after 2006 are from RCP4.5 scenario
EP	Early period experiment	climatological temperature and salinity flux corrections from relaxation run	Climatological EP GHG (1964-1981) and EP AA(1970-1981)　precursor emissions
PD-ALL	Present day all forcing experiment	same as above	Climatological PD GHG and PD AA precursor emissions
PD-GHG	Present day GHG forcing	same as above	Climatological PD GHG and EP AA precursor emissions
PD-AA	Present day AA forcing	same as above	Climatological EP GHG and PD AA precursor emissions

776

777

778
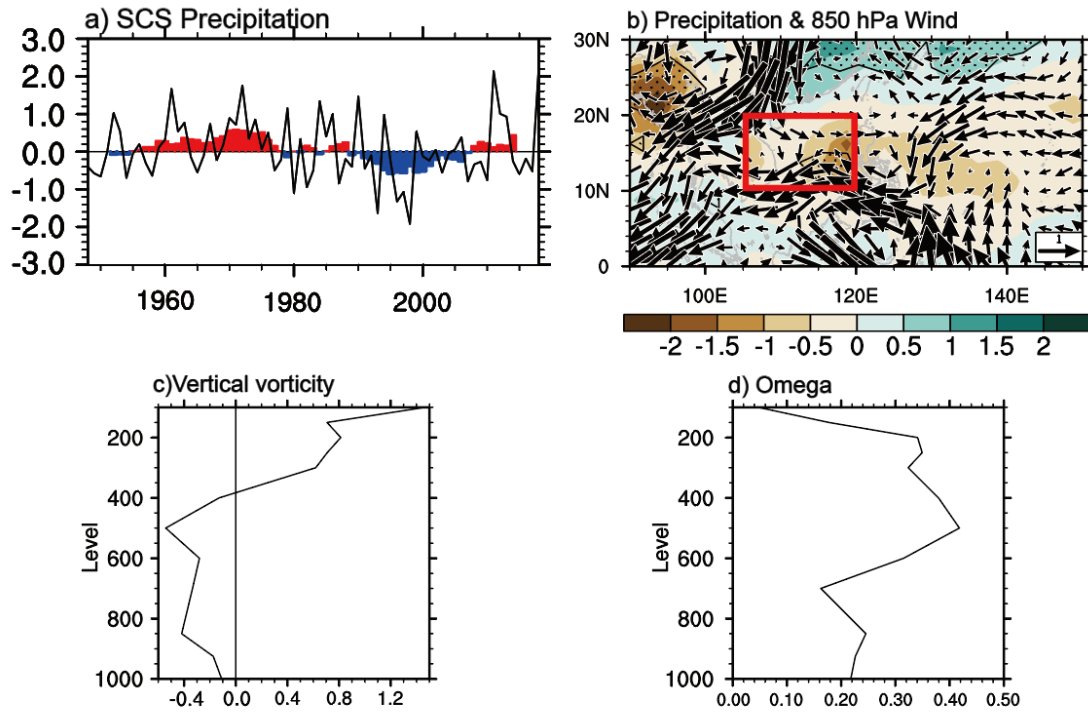
Fig.1 a) Time series (line) and 9 years moving mean (color bar) of (June-July-August) JJA

mean precipitation (mm day^{-1}) over the South China Sea region (10°N-20°N,105°E-120°E)

based on NOAA_PREC data set. b)-d) changes between present day (1994-2011) and

early period (1964-1981).

b) Precipitation (mm/day) of NOAA_PREC and 850hPa wind(m/s) of NCEP reanalysis.

Changes of precipitation in slash regions are statistically significant at the 10% level using

a two-tailed Student's t-test.

c) Vertical profile of vorticity (10^{-6}/s) over the SCS region, d) profile of vertical velocity

(Omega, hPa/s) in pressure coordinate over the SCS. Red box highlights the SCS region.

788

789
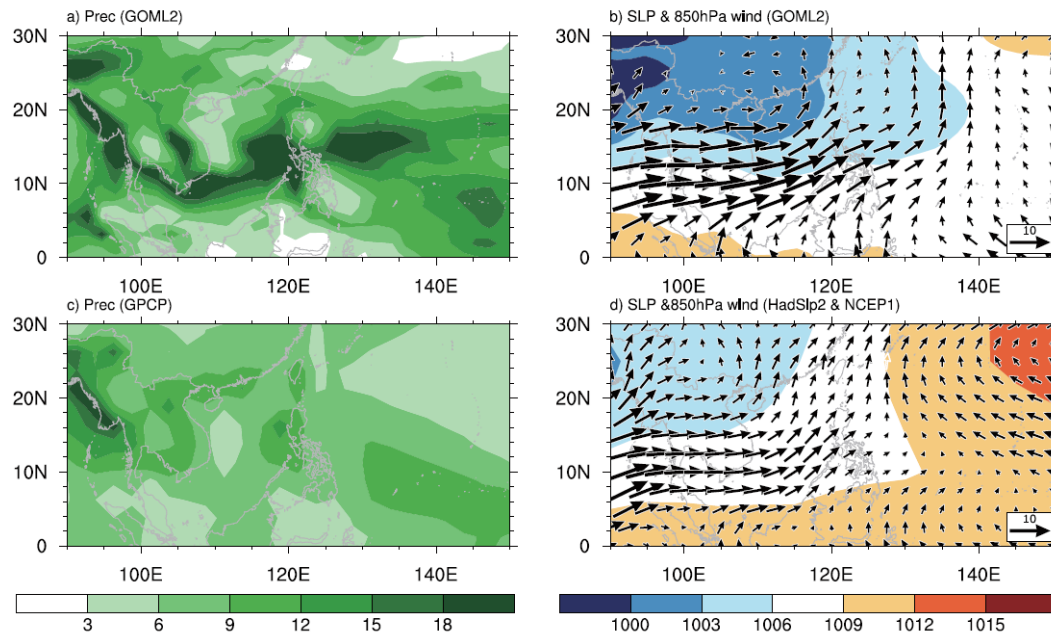
790　Fig.2 Present day (1994-2011) climatological precipitation (mm/day), sea level pressure

791　(hPa), and 850hPa wind(m/s) in JJA. a) and b) GOML2 simulation.

792　c) and d) GPCP precipitation, HadSLP2 SLP, and NCEP reanalysis 850 hPa wind.

793

a) Prec, 500hPa Omega & 850hPa Wind (GHG & AA)

b) Prec, 500hPa Omega & 850hPa Wind (GHG)

c) Prec, 500hPa Omega & 850hPa Wind (AA)
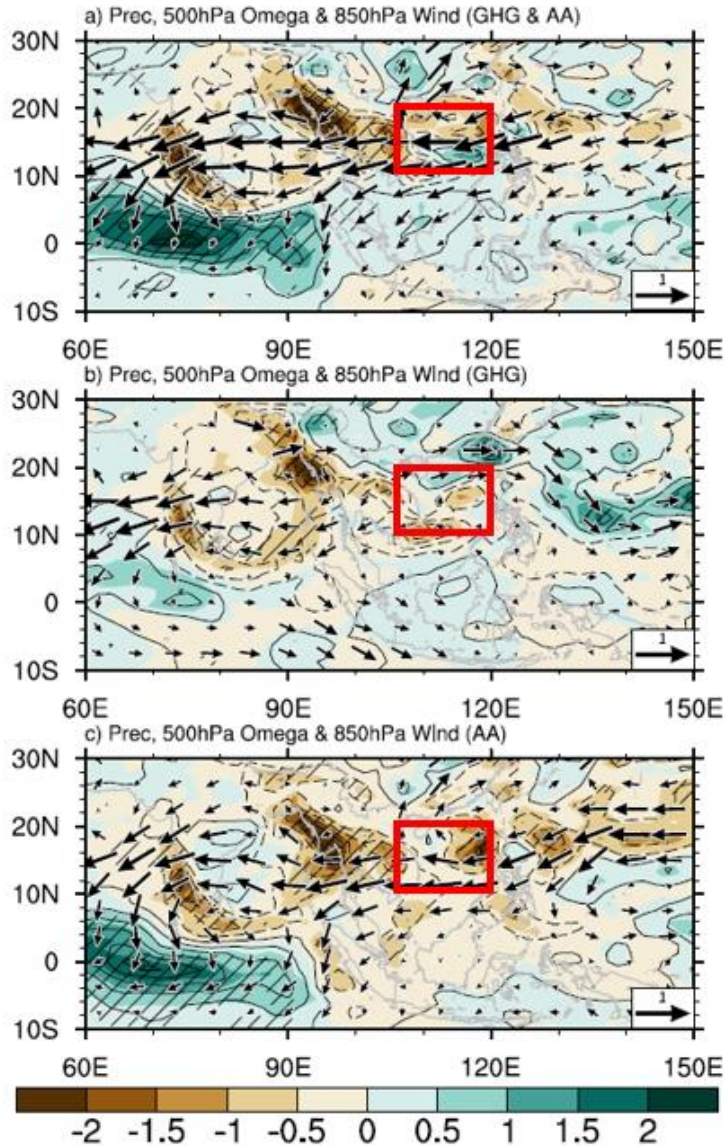
794

795 Fig.3 Simulated changes of precipitation (shade, mm/day), 500hPa Omega (contour,

796 0.01Pa/s) and 850hPa wind (vector, m/s) in JJA. a) Response to anthropogenic forcing

797 (PD-ALL minus EP), b) response to GHG forcing (PD-GHG minus EP), and c) response to

798 AA forcing (PD-AA minus EP) Changes of precipitation in slash regions are statistically

799 significant at the 10% level using a two-tailed Student's t-test. Red box highlights the SCS

800 region.
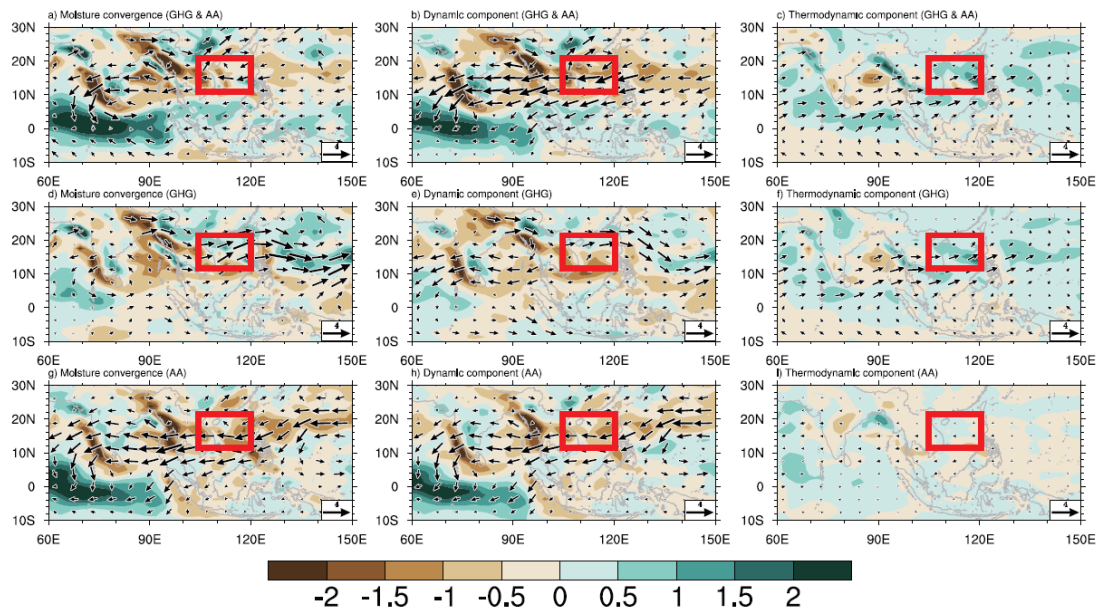
Fig.4. Simulated changes of vertically integrated moisture flux transport (kg/m*s) and its convergence (mm/day) in JJA between PD and EP of All forcing (a, b, c), GHG forcing (d, e, f), and AA forcing (g, h, f). (a, d, g) total moisture flux and its convergence. (b, e, h) dynamic components related to changes in circulation. (c, f, i) thermodynamic components related to changes in humidity. Red box highlights the SCS region.

810
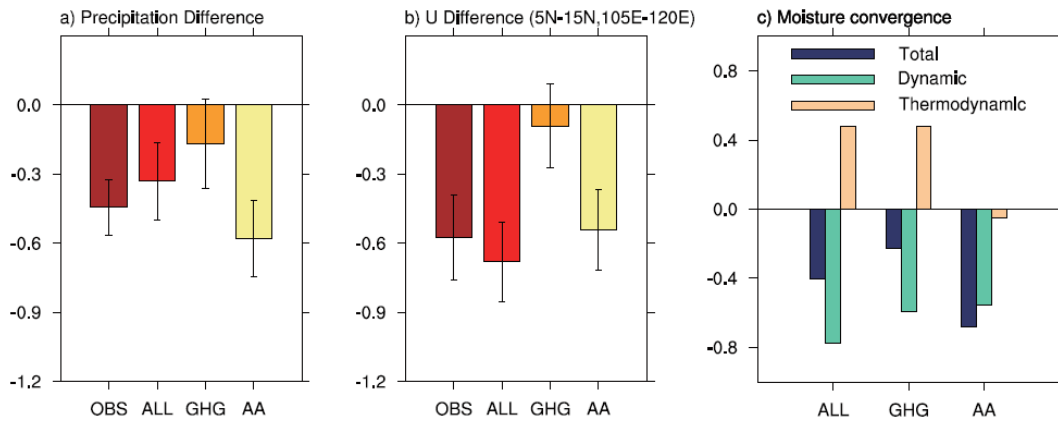
811

812 Fig.5 a) precipitation (mm/day) change between PD and EP in observations

813 (NOAA_PREC), all forcing, GHG forcing and AA forcing over the SCS region (10°N-

814 20°N,105°E-120°E) in JJA.

815 b) zonal wind (m/s) change between PD and EP in observations (NCEP reanalysis 1), all

816 forcing, GHG forcing and AA forcing over south SCS region (5°N-15°N,105°E-120°E) in

817 JJA. The error bars indicate the standard errors of the mean difference。

818 c) simulated change of vertically integrated moisture transport convergence (blue, mm/day)

819 between PD and EP in all forcing, GHG forcing and AA forcing over SCS region (10°N-

820 20°N,105°E-120°E) in JJA. Green bars and yellow bars are the same as blue bars but for

821 dynamic component and thermodynamic component of moisture convergence.

822

823

a) Velocity_potential & divergent wind (850hPa)

b) Velocity_potential & divergent wind (200hPa)

824
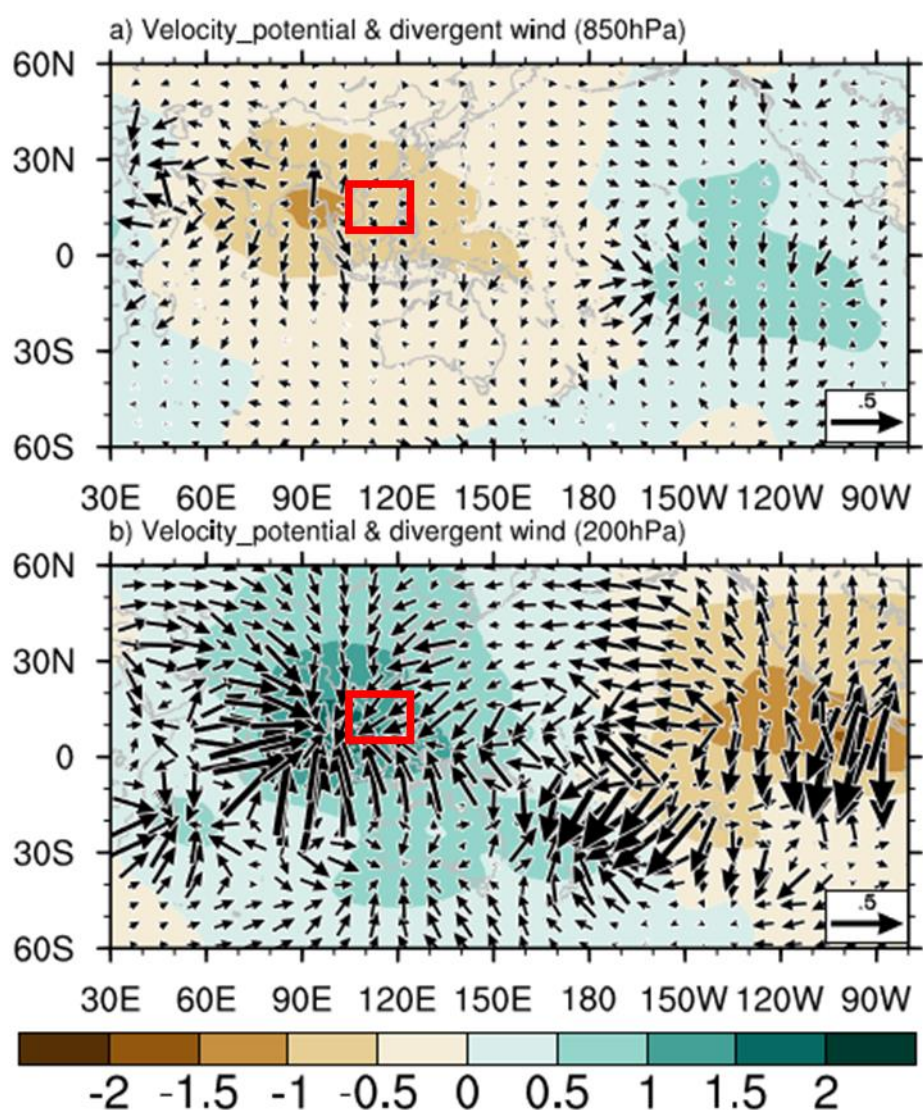
825   Fig.6 Simulated changes in velocity potential (shaded, 10^5 m^2/s) and divergent wind

826   (vectors m/s) in JJA in response to GHG forcing (PD-GHG minus EP).   a) at 850hPa,

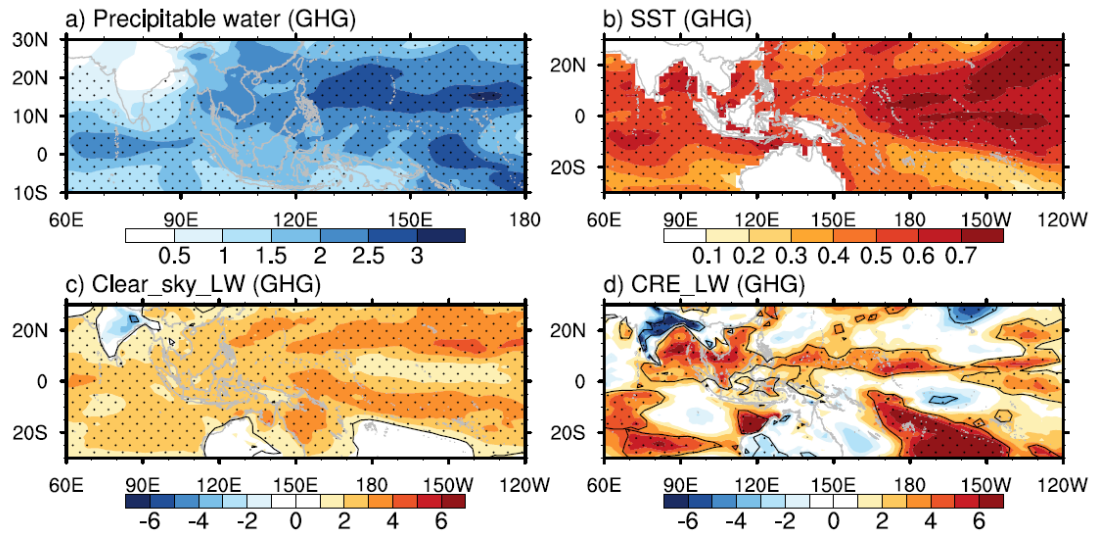827   and b) at 200hPa. Red box highlights the SCS region.

828

829

830

Fig.7 Simulated changes in JJA between PD and EP in response to GHG forcing. a)

precipitable water (kg/m²), b) sea surface temperature (℃), c) surface clear sky net

longwave radiation (W/m²), and d) cloud radiative effect of longwave radiation (W/m²).

Radiations are positive downward. Dot regions are statistically significant at the 10% level

using a two-tailed Student's t-test.

836

Zonal mean (60° E-150° E) of JJA (AA)

a) meridional circulation

b) SST

837
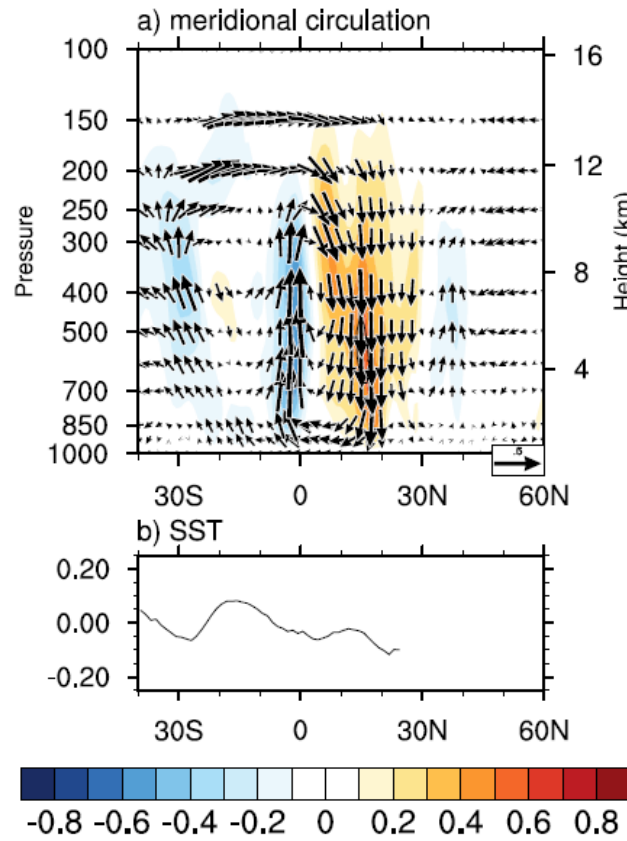
Fig.8 Simulated changes in JJA between PD and EP in response to AA forcing.   a) zonal

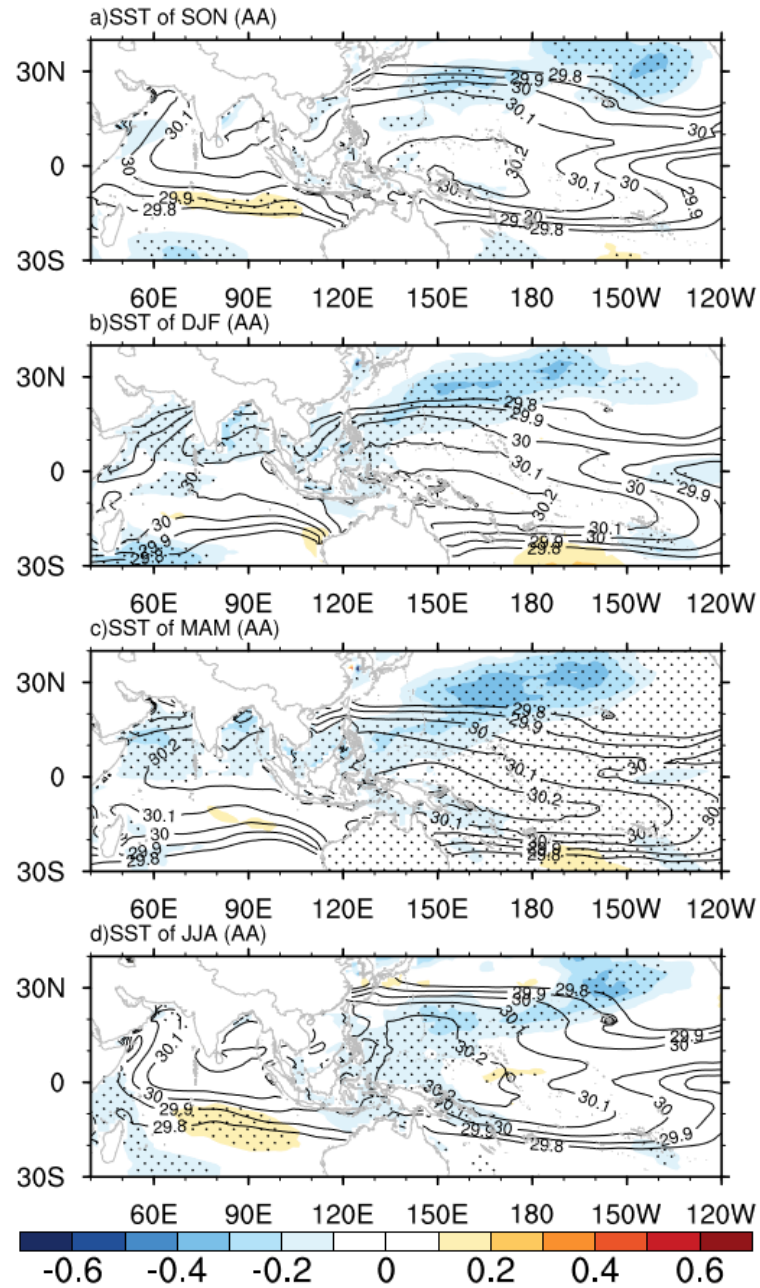mean meridional circulation(vector) and vertical velocity(contour). Unit of meridional wind:

m/s, unit of vertical wind :0.01Pa/s.
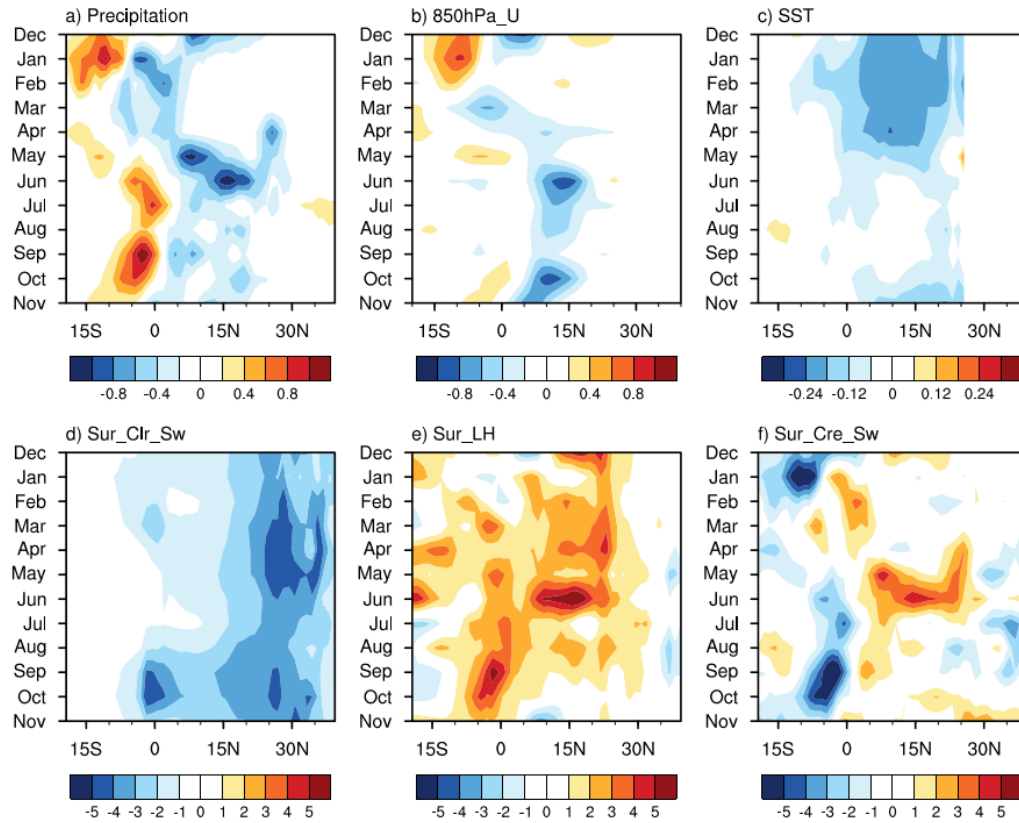
b) zonal mean sea surface temperature (℃).

842

843

Fig.9 Simulated seasonal changes (color, ℃) in sea surface temperature between PD
and EP in response to AA forcing and corresponding climatology (contour, ℃) in the EP
experiment. a) boreal autumn (SON), b) winter (DJF), c) spring (MAM), and d) JJA. Dot
regions are statistically significant at the 10% level using a two-tailed Student's t-test.

Fig.10 Simulated seasonal evolutions of zonal averaged changes over the sector (60°E-150°E) between PD and EP in response to AA forcing. a) precipitation change (mm/day) b)850hPa zonal wind(m/s), c) sea surface temperature(℃), d) surface clear sky net short wave radiation, e) surface latent heat flux(W/m²), and f) surface cloud radiation effect of short wave radiation (W/m²). Radiation and flux are positive downward.

855

856
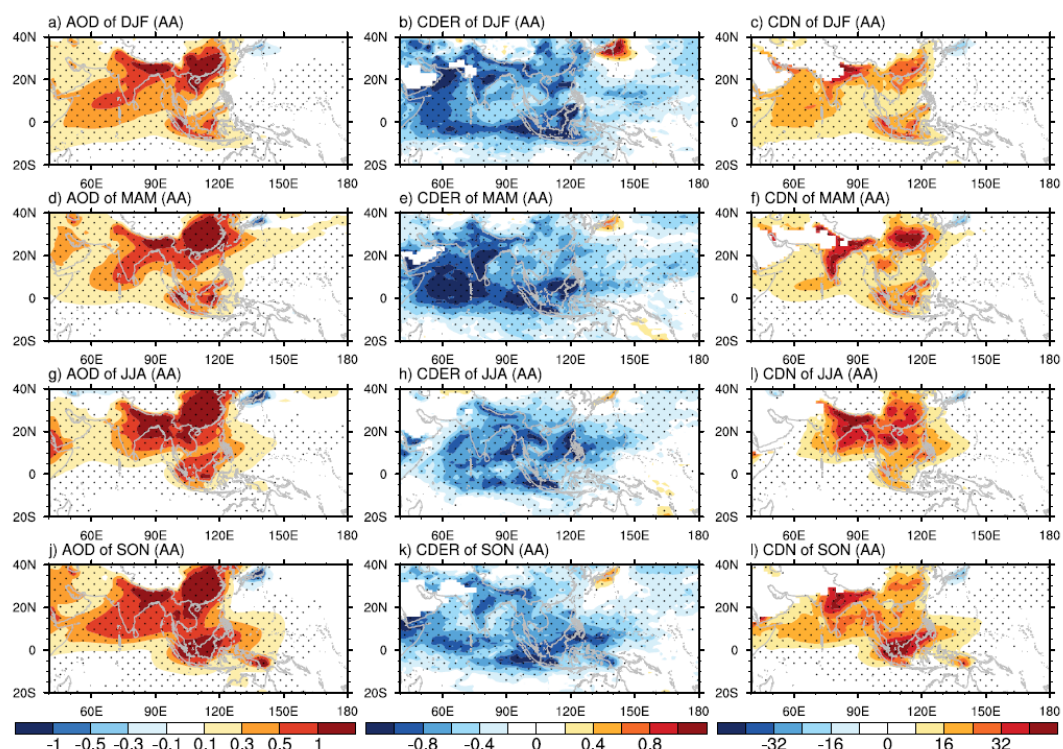
Fig.11 Simulated seasonal changes of aerosol optical depth (AOD, left panels, unit in 0.1) at 0.55 um, cloud droplet effective radius (CDER, middle panels, unit in um) and cloud droplet number (CDN, right panels, unit in 10^9 m^{-2}) between PD and EP in response to AA forcing. a)-c) DJF. d)-f) MAM, g)-h) JJA, j)-l) SON.

861